A Phase Shifter with One Tunable Component for a Reflectarray Antenna

O. G. Vendik[1] and M. Parnes[2]

[1]St. Petersburg Electrotechnical University, Russia
E-mail: OGVendik@mail.eltech.ru

[2]MPA, Israel
E-mail: Michael@mpa.co.il

Abstract

The combination of a dipole and a tunable varactor forms a phase shifter with one tunable component that provides a phase shift over a wide range, from 0° to nearly 360°. The dipole, loaded with a tunable varactor, is used as a patch component of a low-profile reflectarray antenna. An economic assessment shows that the production price of the suggested phase shifter with one tunable component is more than 10 times smaller than the price of the traditional phase shifter, based on p-i-n diode components. The design of such a phase shifter is the goal of this paper. Simulations of the phase shift and loss of the reflected wave as a function of control voltage applied to the varactor were used, based on an analytical model verified by full-wave analysis. The results of simulations are in agreement with measurements. The fast and correct simulation of the reflection coefficient from the dipole loaded with the tunable varactor can be used for the design and optimization of a low-profile steerable reflectarray antenna.

Keywords: Antenna arrays; beam steering; electromagnetic reflection; microstrip antennas; microstrip arrays; microwave antenna arrays; millimeter wave antennas; phase shifters; phased arrays; planar arrays; radar antennas; reflector antennas; scanning antennas; varactor tuners

1. Introduction

A low-profile reflectarray antenna consists of rectangular microstrip-patch radiators. The patch radiators form a set of reflectors that convert a spherical wave radiated by a primary radiator into a plane wave (Figure 1). The phase shifts of the waves reflected by different radiators are specified to convert the spherical wave into the plane wave. In order to exclude large phase incursions, the principle of the Fresnel mirror is used.

There is a lot of experience in designing low-profile reflectarray antennas [1-6]. A tunable reflectarray can be formed by a set of dipoles loaded with tunable varactors, which can be realized as semiconductor or ferroelectric devices [7]. A dipole loaded with a varactor is shown schematically in Figure 2. In Figure 3, one can see a fragment of the reflectarray surface covered by the set of dipoles loaded with tunable varactor diodes. A set of versions of tunable antenna structures, based on RF MEMS switches, semiconductor, or ferroelectric-tunable components, has been described [8-16].

A combination of a dipole and a tunable varactor forms a phase shifter with one tunable component that provides a phase shift over a wide range, from 0° to 360°. The design of such a phase shifter is the goal of this paper. The characterization of any type of phase shifter is given by the figure of merit (FM) of the phase shifter. The numerical value of the figure of merit is determined by the commutation quality factor (CQF) of the tunable component (the varactor) [17]. The general relationship between the figure of merit and the commutation quality factor was discussed earlier for the example of a phase shifter with a ferroelectric tunable component [18]. Such a procedure for characterizing the phase shifter will be used for the phase shifter with one tunable component to which this paper is dedicated.
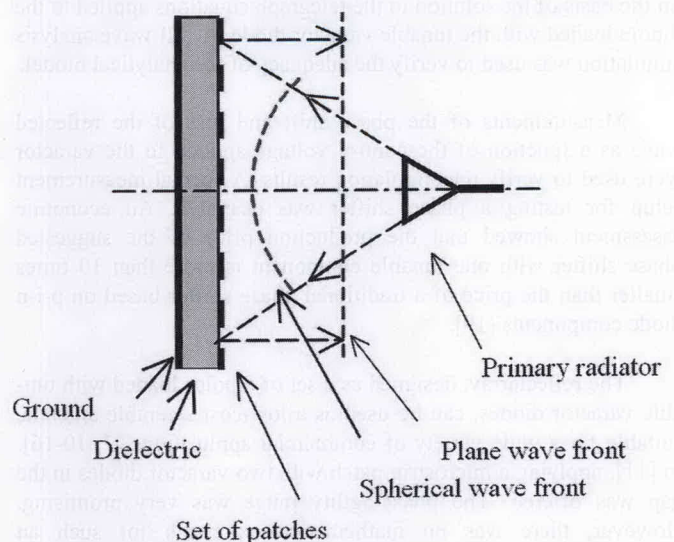

Figure 1. A schematic of the low-profile reflectarray antenna consisting of rectangular microstrip-patch radiators.
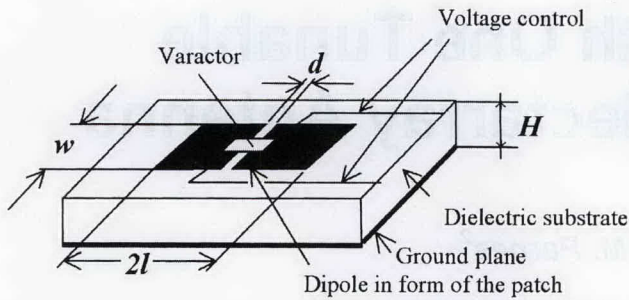
Labels in figure: Primary radiator; Ground; Dielectric; Set of patches; Plane wave front; Spherical wave front

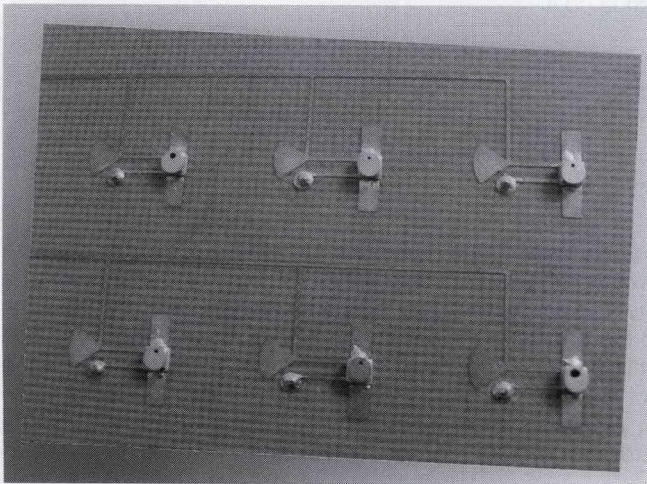**Figure 2. A sketch of the dipole loaded by the tunable varactor.**

Figure 3. A photo of a part of the reflectarray surface, covered by the set of dipoles loaded by the tunable MA46H70 varactor.

The design of an antenna array is based on modeling the elementary equivalent waveguide cell containing a patch radiator at the interface between free space and the grounded substrate layer. The fundamental task of the problem discussed is to develop a procedure for the calculation of the reflection coefficient of a linearly polarized wave that is normally incident upon the patch radiator. An analytical-model approach to the problem has been developed on the basis of the solution to the telegraph equations applied to the dipole loaded with the tunable varactor diode. A full-wave analysis simulation was used to verify the adequacy of the analytical model.

Measurements of the phase shift and loss of the reflected wave as a function of the control voltage applied to the varactor were used to verify the simulation results. A special measurement setup for testing a phase shifter was designed. An economic assessment showed that the production price of the suggested phase shifter with one tunable component is more than 10 times smaller than the price of a traditional phase shifter based on p-i-n diode components [19].

The reflectarray, designed as a set of dipoles loaded with tunable varactor diodes, can be used as a low-cost steerable antenna, suitable for a wide variety of commercial applications [7, 10-16]. In [11], applying a microstrip patch with two varactor diodes in the gap was offered. The phase-agility range was very promising. However, there was no mathematical approach for such an antenna-design methodology. The authors of [13] offered a radiating patch aperture-coupled to a transmission line loaded with two varactor diodes. A very interesting solution was described in [12].

However, since it was not a full planar structure, the surface-mounting technology of the varactor was inapplicable, and therefore this solution might be quite costly for complex phased arrays.

2. Fundamentals of the Phase Shifter with One Tunable Component

2.1 Theory

The equivalent presentation of a reflection-type phase shifter is shown in Figure 4. Parallel and series versions of the resonant circuit can be considered with equal correctness. An ideal impedance transformer can be included between the transmission line with characteristic impedance Z_0 and the resonant circuit. The theory applied for the series circuit will be considered. The duality principle should be used to transform formulas for the parallel-resonant circuit into formulas for the series-resonant circuit.

The impedance of the circuit shown in Figure 4a can be written as follows:

$$Z(f,q) = iX_0 \frac{f}{f_0} - iX_0 \frac{f_0}{f} \frac{2q}{n+1} + R, \qquad (1)$$

where q is the tuning parameter; n is the tunability of the capacitor, $1 \le q \le n$; and f_0 is the center frequency. The components of the schematic shown in Figure 4a are included in Equation (1) by the following relations:

$$L_0 = \frac{X_0}{2\pi f_0},$$
$$\qquad (2)$$
$$C(q) = \frac{1}{2\pi X_0 f_0} \frac{n+1}{2q},$$

$$n = \frac{C_{max}}{C_{min}},$$

$$C_{max} = C(1), \qquad (3)$$

$$C_{min} = C(n).$$
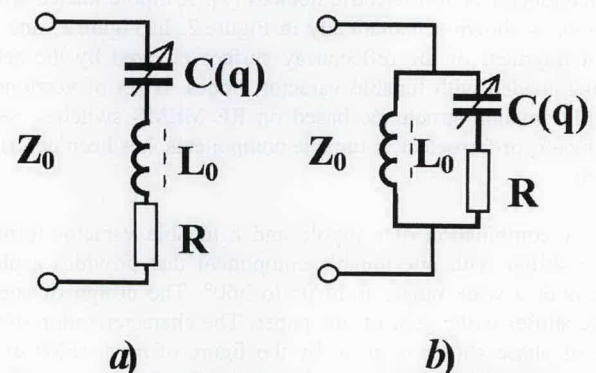

a)   *b)*

Figure 4. Simplified schematics of a reflect-type phase shifter.

The reflection coefficient for the circuit (Figure 4a) can now be presented as follows:

$$\Gamma(f,q) = |\Gamma(f,q)| e^{i\varphi(f,q)} = \frac{Z(f,q)-Z_0}{Z(f,q)+Z_0}. \tag{4}$$

From Equation (4), one obtains the modulus of the reflection coefficient,

$$|\Gamma(f,q)| = \sqrt{\frac{\{\operatorname{Im}[Z(f,q)]\}^2 + \{Z_0 - \operatorname{Re}[Z(f,q)]\}^2}{\{\operatorname{Im}[Z(f,q)]\}^2 + \{Z_0 + \operatorname{Re}[Z(f,q)]\}^2}}, \tag{5}$$

and the phase shift of the reflected wave with respect to the incident wave:

$$\varphi(f,q) = 2\arctan\{\operatorname{Im}[Z(f,q)/Z_0]\}. \tag{6}$$

The last equation is correct for the case $\operatorname{Re}[Z(f,q)] \ll Z_0$. The loss of the reflection-type phase shifter is defined as

$$L(f,q) = -20\log[|\Gamma(f,q)|] \text{ [dB]}. \tag{7}$$

In Figure 5, the phase shift and loss are shown as functions of tuning factor, q, for different frequencies, f. As examples, the following parameters of the model were used: $n=4$, $Z_0 = 50$ ohms, $X_0 = 400$ ohms, $R = 10$ ohms, $f = 9$ (case 1), 10 (case 2), and 11 (case 3) GHz.

The phase difference, maximum loss, and reactance at the edges of the tuning range are given by Equations (8)-(10), respectively:

$$\delta\varphi_{max} = \varphi(f_0, n) - \varphi(f_0, 1), \tag{8}$$

$$L_{max} = L\left(f_0, \frac{n+1}{2}\right), \tag{9}$$

$$X_1(f) = \operatorname{Im}[Z(f,1)],$$
$$X_2(f) = \operatorname{Im}[Z(f,n)]. \tag{10}$$

One can suppose the requirement that the maximum phase difference and the maximum loss do not depend on the frequency in a frequency range of about 20%. At the frequency $f = f_0$, one obtains from Equation (1)

$$X_1(f_0) = -X_2(f_0) = X_0 \frac{n-1}{n+1}. \tag{11}$$

Combining Equations (6), (8), and (11), one obtains

$$\delta\varphi_{max} = 4\arctan\left(\frac{X_0}{Z_0}\frac{n-1}{n+1}\right). \tag{12}$$

For $\operatorname{Re}[Z(f,q)] \ll Z_0$ and $f = f_0$, Equations (7) and (9) give

$$L_{max} = 8.68\frac{2R}{Z_0}. \tag{13}$$

On the basis of Equation (12), Equation (13) can be rewritten in the following form:

$$L_{max} = 8.68\frac{2R}{X_0}\frac{n+1}{n-1}\tan\left(\frac{\delta\varphi_{max}}{4}\right). \tag{14}$$

2.2 Figure of Merit of the Phase Shifter

The figure of merit (FM) is defined as follows:
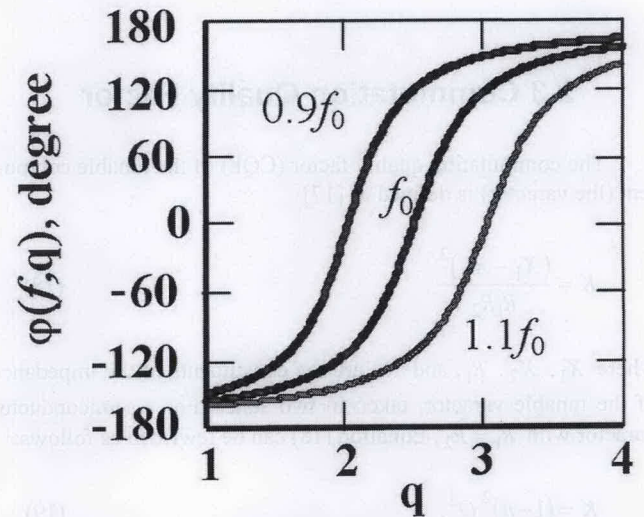
$$F = \frac{\Delta\varphi}{L}, \tag{15}$$

Figure 5a. The phase shift of the reflected wave with respect to the incident wave as a function of the tuning factor, q, for different frequencies $f_0 \pm 10\%$.
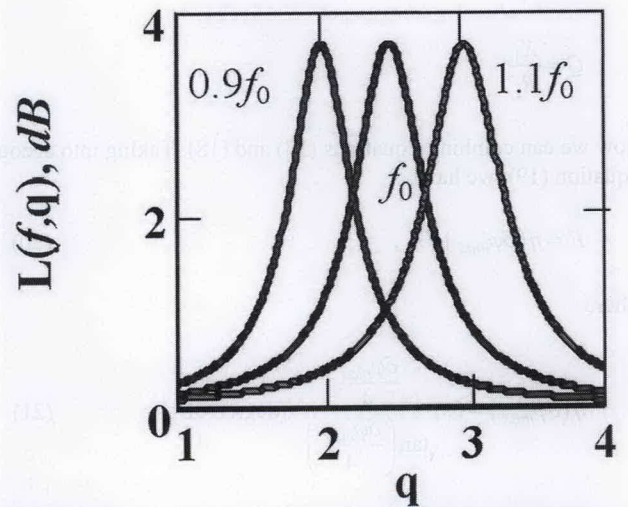

Figure 5b. The loss of the reflected wave with respect to the incident wave as a function of the tuning factor, q, for different frequencies $f_0 \pm 10\%$.

where $\Delta\varphi$ is the phase shift in degrees; for a reflection-type phase shifter, L is the loss in dB.

Thus, in accordance with Equations (14) and (15), one may write the figure of merit of the phase shifter in degree/dB as follows:

$$F = \frac{4}{8.68}\frac{180}{\pi}\frac{X_0}{2R}\frac{n-1}{n+1}\frac{\frac{\delta\varphi_{max}}{4}}{\tan\left(\frac{\delta\varphi_{max}}{4}\right)}. \tag{16}$$

Comparing Equations (13) and (16), one obtains

$$F = \frac{1}{8.68}\frac{180}{\pi}\frac{X_1-X_2}{R}\frac{\frac{\delta\varphi_{max}}{4}}{\tan\left(\frac{\delta\varphi_{max}}{4}\right)}. \tag{17}$$

2.3 Commutation Quality Factor

The commutation quality factor (CQF) of the tunable component (the varactor) is defined as [17]

$$K = \frac{(X_1-X_2)^2}{R_1 R_2}, \tag{18}$$

where X_1, X_2, R_1, and R_2 are the constituents of the impedance of the tunable varactor, taken in two states. For a semiconductor varactor with $R_1 = R_2$, Equation (18) can be rewritten as follows:

$$K = (1-n)^2 Q^2, \tag{19}$$

where

$$n = \frac{X_1}{X_2},$$

$$Q = \frac{X_1}{R_1}.$$

Now we can combine Equations (17) and (18). Taking into account Equation (19), we have

$$F = \eta\left(\delta\varphi_{max}\right)\sqrt{K}, \tag{20}$$

where

$$\eta\left(\delta\varphi_{max}\right) = 6.6\frac{\frac{\delta\varphi_{max}}{4}}{\tan\left(\frac{\delta\varphi_{max}}{4}\right)} \text{ [degree/dB]}. \tag{21}$$

Figure 6 presents the factor η as a function of the maximum phase difference in the frequency range of 9 to 11 GHz. It is important to stress that for $\delta\varphi_{max} \to 360°$, Equation (14) gives $L_{max} \to \infty$ and Equation (21) gives $\eta\left(\delta\varphi_{max}\right) \to 0$. Consequently, $\delta\varphi_{max} = 360°$ cannot be realized. For $\delta\varphi_{max} = 300°$, one obtains $\eta(300) = 2.2$.

In accordance with Equations (20) and (21), for $\delta\varphi_{max} = 300°$ one obtains the figure of merit of the phase shifter as follows:

$$F = 2.2\sqrt{K}. \tag{22}$$

A semiconductor varactor can be characterized by the tunability, $n = 5$ to 6, and the quality factor at a frequency of 10 GHz, $Q = 6$ to 8 [17, 19]. Thus in accordance with Equation (19), the commutation quality factor of a semiconductor varactor at $f = 10$ GHz can reach $K \cong 1000$. In accordance with Equation (22), one has $F \cong 75$ deg/dB. In the case of $\delta\varphi_{max} = 300°$, that gives a maximum loss $L_{max} = 4$ dB.

Let us exclude the factor q from Equations (6) and (7), and obtain the dependence of loss on the value of the phase shift. Combining the phase shift and loss presented in Figure 5 and defined by Equations (6) and (7), we can find the insertion loss of the phase shifter as a function of the phase shift. The result of the simulation is shown in Figure 7.

The equations for the figure of merit of different versions of microwave phase shifters were developed in [17, 18]. It is known that for a phase shifter in the form of a transmission line with tunable phase velocity,
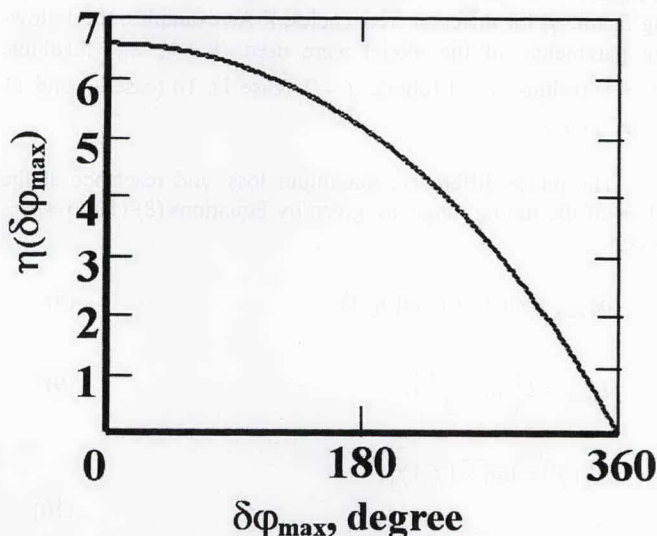

Figure 6. The factor η in the formula for the figure of merit of the reflection-type phase shifter with one tunable component as a function of the maximum phase difference, $\delta\varphi_{max}$.
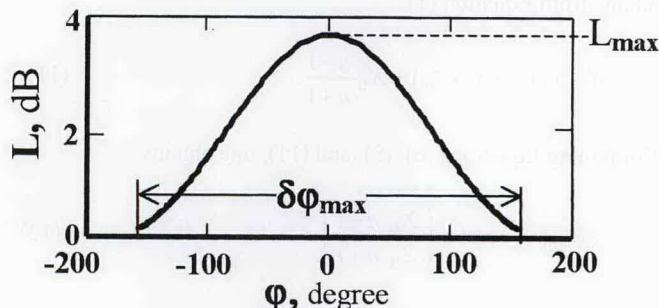

Figure 7. The loss of the reflection-type phase shifter with one tunable component as a function of the maximum phase difference, $\delta\varphi_{max}$.

$$F = 6.6\sqrt{K} . \tag{23}$$

For a digital phase shifter with more than three bits, one has

$$F = 8.35\sqrt{K} . \tag{24}$$

In addition to the known formulas of Equations (22) and (23), Equation (24) widens the characterization of the figure of merit applied to the microwave phase shifters of different types.

2.4. Characteristic Features of the Reflection-Type Phase Shifter with One Tunable Component

The following features characterize the phase shifter considered:

1. Increasing the phase shift is followed by increasing the loss. The reasonable maximum tunable phase shift is taken to be 300°, which is quite enough for designing a reflectarray antenna.

2. In the process of beam steering, the phases of different radiators are distributed over the reflectarray antenna's surface. Hence, the loss can be averaged over the reflectarray antenna. In accordance with Figure 6, the averaged loss can be taken approximately as half the maximum loss.

3. The commutation quality factor of the varactor used in the phase shifter with only one tunable component is required to be higher than the commutation quality factor of the tunable components of traditional phase shifters [17, 18].

3. A Model of an Array Formed by a Set of Tunable Reflecting Components

In order to simplify the theory of the tunable array, we suppose that the mutual influence between the radiators is neglected. That can be justified, to a considerable extent, by the absence of periodic phase distributions along the array. The absence of the phase periodicity is explained by predetermination of the array to transform a spherical phase front into a plane phase front [20]. Therefore, one may separately calculate the reflection from any dipole belonging to the array.

Figure 8 illustrates the decomposition of the array into a set of virtual waveguides. Each waveguide is an element of an infinite array. A virtual waveguide is formed by "electric" and "magnetic" walls. Electric field lines are normal to the "electric" walls, and magnetic field lines are normal to the "magnetic" walls. Such a distribution of the field corresponds to the T_{00} waveguide mode. The subscripts "00" are used to stress that electric and magnetic fields do not depend on the coordinates in the cross section of the virtual waveguide considered.

One tunable dipole is situated inside the virtual waveguide. The schematic diagram for the positioning of the dipole loaded

with the tunable varactor is shown in Figure 9. Let us use the plane in which the dipole is situated as a reference plane for the definition of the phase of the reflection coefficient. In the reference plane, the dipole and the section of the waveguide between the dipole and the ground plane are included in parallel. The impedance of this parallel junction determines the reflection coefficient, $\Gamma(f, U)$, in which we are interested. It is easy to calculate the input impedance of a waveguide section. It is much more complicated to find the impedance of the waveguide containing the dipole loaded with the tunable varactor.

4. An Analytical Model of the Dipole Loaded by a Tunable Varactor

An analytical model represents a set of simple formulas that make it possible to simulate the impedance of the dipole as a function of frequency, dimensions, the position towards the waveguide walls, and the capacitance of the included varactor. The analytical model is based on an approximate method of simulation. The simulation is very fast, and can be used for optimization of the structure. Using the analytical model makes it possible to obtain a first approximation of the design.
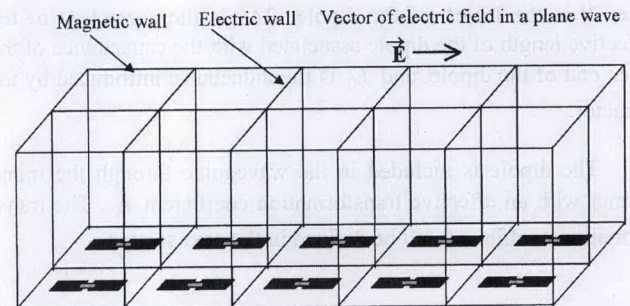
Figure 8. The decomposition of the array into a set of virtual waveguides. A virtual waveguide is formed by "electric" and "magnetic" walls.
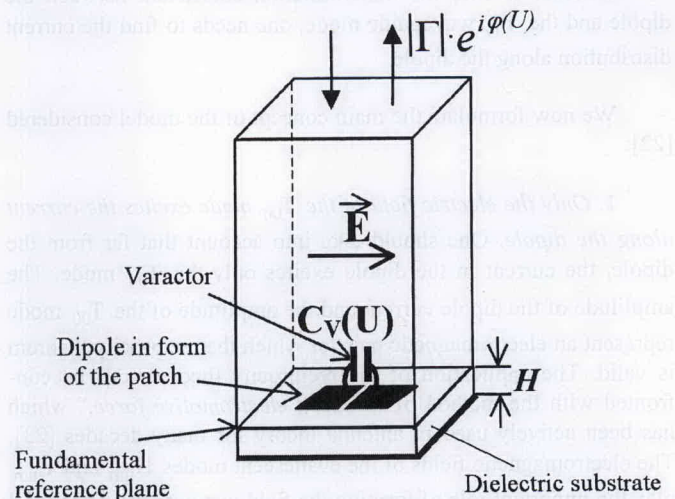
Figure 9. The position of the dipole loaded with the tunable varactor in the virtual waveguide.

4.1 Equivalent Circuit of the Dipole

A tunable varactor with capacitance (C_v) is included in the center of each dipole (Figure 9). A microstrip-line section, situated on the dielectric substrate with a perfect ground plane, represents the dipole loaded with the tunable capacitor. We consider the effective dielectric constant and the characteristic impedance of the microstrip-line section forming the dipole [21]:

$$\varepsilon_{eff} = \frac{\varepsilon_d + 1}{2} + \frac{\varepsilon_d - 1}{2\sqrt{1 + 10H/w}}, \tag{25}$$

$$Z_B = \frac{120\pi/\sqrt{\varepsilon_{eff}}}{\frac{w}{H} + 3.42 - 2.44\frac{H}{w} + \left(\frac{H}{w}\right)^2}, \tag{26}$$

where H is the substrate thickness and w is the width of the dipole. The impedance of the dipole loaded with C_v (we consider two halves of the dipole connected in series) is

$$z_D(f, C_v) = -i2Z_B \cot k_B(l + \Delta l) + \frac{1}{i\omega C_v} + r + i\omega L_0, \tag{27}$$

where r is the resistance responsible for loss in the capacitor and the dipole, $k_B = 2\pi/\lambda_B$, λ_B is the wavelength in the microstrip line, $2l$ is the length of the dipole, $2\Delta l$ is the correction of the effective length of the dipole associated with the capacitance of the open end of the dipole, and L_0 is the inductance introduced by the varactor.

The dipole is included in the waveguide through the transformer with an effective transformation coefficient n_0. The transformation coefficient will be defined in the next section.

4.2 The Transformation Coefficient Between the Dipole and the T_{00} Waveguide Mode

In order to find the transformation coefficient between the dipole and the T_{00} waveguide mode, one needs to find the current distribution along the dipole.

We now formulate the main concept of the model considered [22]:

1. *Only the electric field of the* T_{00} *mode excites the current along the dipole.* One should take into account that far from the dipole, the current in the dipole excites only the T_{00} mode. The amplitude of the dipole current and the amplitude of the T_{00} mode represent an electromagnetic pair for which the reciprocity theorem is valid. The application of the reciprocity theorem can be confronted with the method of "*induced electromotive force*," which has been actively used in antenna theory for many decades [23]. The electromagnetic fields of the evanescent modes H_{nm} and E_{nm} play the important role of forming the field just near the dipole and the current distribution along the dipole.

2. *The current distribution along the dipole is determined by the telegraph equations. As an external exciting field in the equation, the electric field of the* T_{00} *mode is used.*

$$\frac{dI(x)}{dx} = -i\omega C_1 U(x),$$

$$\frac{dU(x)}{dx} = -i\omega L_1 I(x) + E_{ext}, \tag{28}$$

where C_1 and L_1 are the capacitance and inductance per unit length of the dipole, and E_{ext} is the electric field of the T_{00} mode just on the dipole. We will use the approximate formulas for the dipole as a microstrip line, Equations (25) to (27), which include the values of C_1 and L_1. Actually, the values of C_1 and L_1 are determined by the energy accumulated by the evanescent modes H_{nm} and E_{nm}.

The coordinates of the dipole (Figure 10) lie in the limits $-l \le x \le l$. The boundary conditions for the solution to Equation (28) are

$$I(l) = 0,$$

$$U(0) = \frac{0.5}{i\omega C_v} I(0), \tag{29}$$

where C_v is the capacitance of the tunable varactor.

The solutions to Equation (28) in the form of the current and voltage as functions of coordinates are shown in Figure 11. The jump of voltage at $x = 0$ is equal to $2U(0)$, and corresponds to the voltage drop on the capacitance of the tunable varactor. Using the Poynting theorem, one can calculate the excitation of current at the dipole by the incident T_{00} wave, and excitation of the T_{00} wave radiated by the dipole. As a result, the transformation coefficient between the dipole and the T_{00} waveguide mode is found:
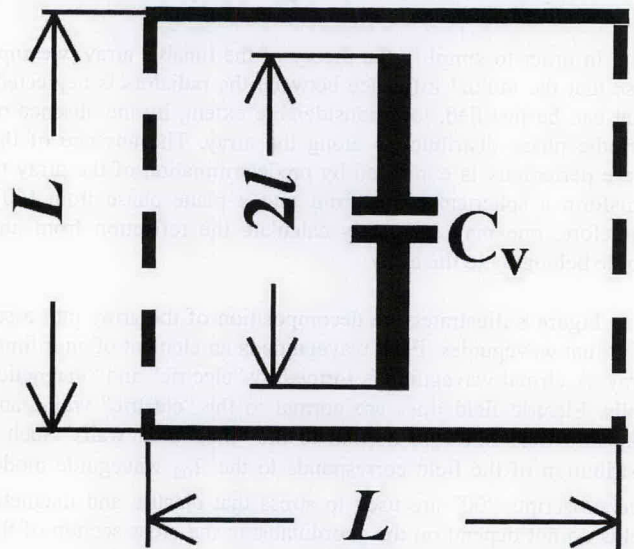

Figure 10. The layout of the dipole loaded by the varactor in the virtual waveguide.
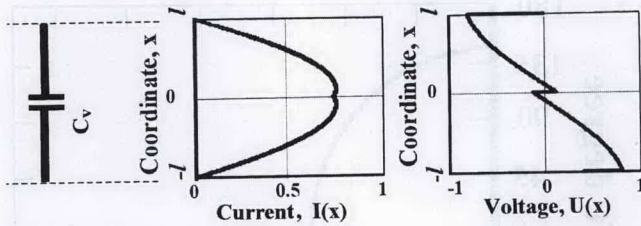
Figure 11. The current and voltage as functions of coordinates along the dipole: solutions to Equation (28).
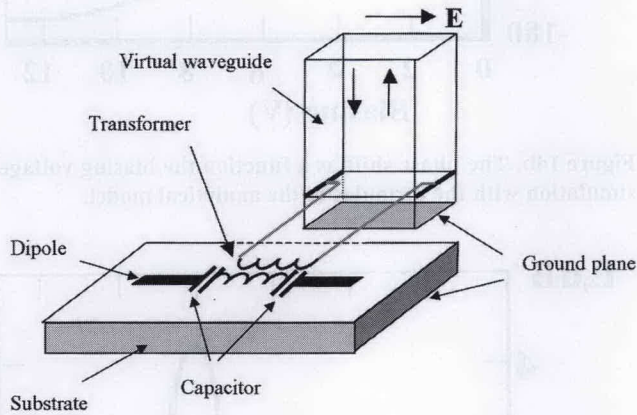

Figure 12. The equivalent circuit of the dipole included in the virtual waveguide.

$$n_0 = \frac{2l}{L}\sqrt{\frac{1}{k_B l}}\sqrt{\frac{1}{k_B l} - \frac{1}{\tan(k_B l)} + \frac{0.5}{\omega C_v Z_B}\left[\frac{\tan(k_B l/2)}{k_B l/2} - 1\right]}.$$

(30)

4.3 The Tunable Reflection Coefficient of the Dipole in the Virtual Waveguide

The equivalent circuit of the dipole included in the virtual waveguide is shown in Figure 12. The admittance of the parallel junction of the dipole and the short-circuited waveguide section is written as follows:

$$Y(f, C_v) = \frac{n_0^2}{z_D(f, C_v)} + \frac{1}{i\frac{Z_0}{\sqrt{\varepsilon_d}}\tan(k_d H)},$$

(31)

where $z_D(f, C_v)$ and n_0 are given by Equations (27) and (30), $Z_0 = 120\pi$ ohms, ε_d is the dielectric constant of the substrate material, H is the thickness of the substrate, and k_d is the wave number of the microstrip-line section forming the dipole.

As was mentioned above, the reference plane is the plane in which the dipole is placed. The reflection coefficient with respect to the reference plane is written as follows:

$$\Gamma(f, C_v) = \frac{Y_0 - Y(f, C_v)}{Y_0 + Y(f, C_v)},$$

(32)

$$Y_0 = Z_0^{-1}.$$

The phase shift in degrees, and the insertion loss in dB, of the phase shifter can then be found:

$$\varphi(f, C_v) = \frac{180}{\pi}\arg\left[\Gamma(f, C_v)\right],$$

(33)

$$L(f, C_v) = -20\log\left[\left|\Gamma(f, C_v)\right|\right].$$

(34)

The result of a simulation of the phase shift as a function of the varactor capacitance for a frequency of 12 GHz is shown in Figure 13. The simulation was done for a dipole with the following dimensions and characteristics: $2l = 8\,\text{mm}$, $w = 3.5\,\text{mm}$, $H = 1.0\,\text{mm}$, $\varepsilon_d = 2.8$, $L = 20\,\text{mm}$, $r = 2.7$ ohms, $\Delta l = 0.525\,\text{mm}$, and $L_0 = 0.07\,\text{nH}$. The parameter Δl was calculated using known microstrip formulas [21]. L_0 was taken as an approximate parameter of the varactor used.

Figure 14a presents the dependence of the varactor capacitance on the biasing voltage. Substituting the dependence of the varactor capacitance on the biasing voltage into Equations (33) and (34), and taking into account the previous simulation, we have found the phase shift and the insertion loss as a function of the biasing voltage (Figure 14b and 14c).
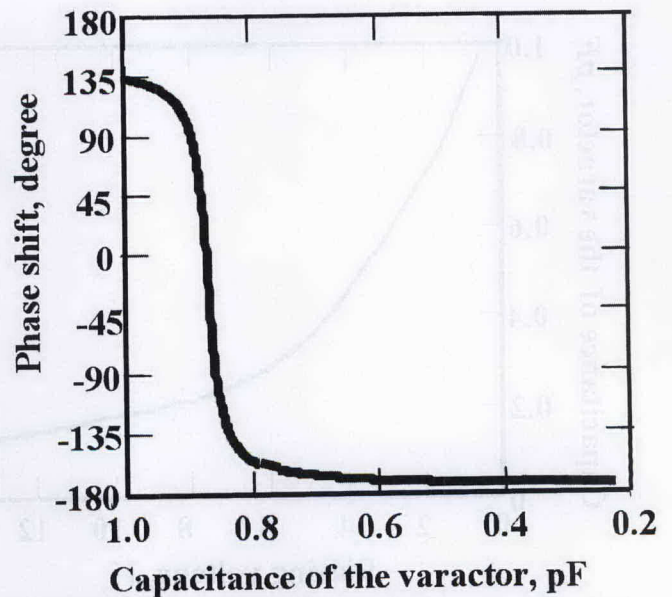

Figure 13. A simulation of the phase shift as a function of the varactor capacitance for a frequency of 12 GHz.

5. Full-Wave Analysis and Experimental Verification

5.1 Verification of the Analytical Model by Simulations Based on a Full-Wave Analysis

In order to verify the analytical model described above, a code based on the Spectral Domain Method of Moments (MoM) was used [24, 25]. Specific entire-domain basis functions were used [26] for the structure of printed transmission lines formed by the dielectric and metal layers. In order to approximate an unknown current density in the dipole, we had to expand components of the current-density vector in a series of chosen basis functions. The Galerkin procedure was implemented to find the vector of unknown basis-function coefficients. The Galerkin procedure made it possible to transform the integral equation with respect to the current-density functions into a system of algebraic equations with respect to the coefficients of the basis functions. The code obtained was efficient because of the combination of a high calculation speed with a highly accurate analysis. The MoM simulation enabled finding the current distribution along the dipole. The dipole is situated in the virtual waveguide section as shown in Figure 9. The reflection coefficient for the T_{00} mode in the virtual waveguide was obtained as a result of simulation. The phase shifts of the reflected wave as a function of the dipole's length for the dipole without a loading capacitor were simulated using the MoM code and the analytical model. The results of the simulation are shown in Figure 15. The phase shift was a function of the dipole's length. The parameters used in the simulations were $f = 25$ GHz; virtual waveguide dimension $L = 6$ mm; width of the dipole $w = 1$ mm; for the substrate, $\varepsilon_d = 2.22$; $H = 0.787$ mm. The small discrepancy between the data obtained from the analytical model and the data of the MoM analysis confirmed that the model parameters Δl and L_0 were correctly defined.

Figure 14b. The phase shift as a function the biasing voltage: a simulation with the formulas of the analytical model.
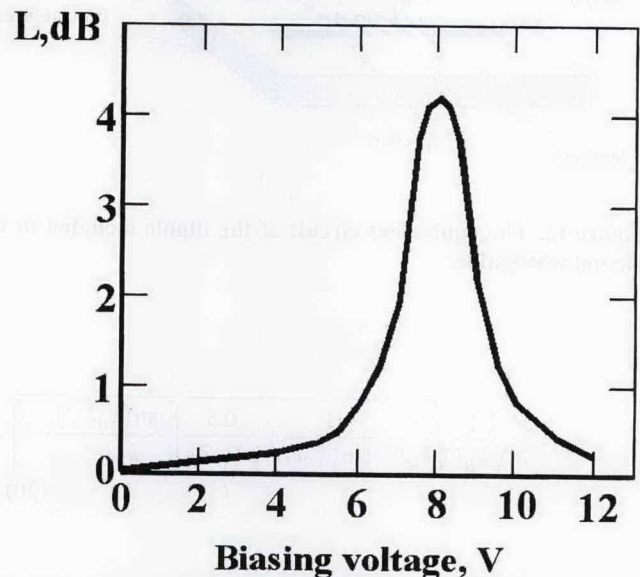
Figure 14c. The insertion loss as a function the biasing voltage: a simulation with the formulas of the analytical model.

5.2 Experimental Investigation of the Reflection-Type Phase Shifter with One Tunable Component

The measurement-setup for measuring the phase shift and insertion loss of the reflection-type phase shifter is shown in Figure 16a. The dipole loaded with the tunable varactor was placed not in the "virtual waveguide" but in a real waveguide with metal walls. The cross section of the waveguide was 18 mm × 23 mm. The TE_{10} waveguide mode was used. Figure 16b presents a photo of the dipole, loaded with the adopted tunable varactor, to be placed in the waveguide with the cross section of 18 mm × 23 mm. The important part of the measurement equipment was the phase meter, which made it possible to obtain the set of the phase and the modulus of the reflected wave. The ratio of the reflected and incident wave moduli determines the insertion loss of the phase shifter.
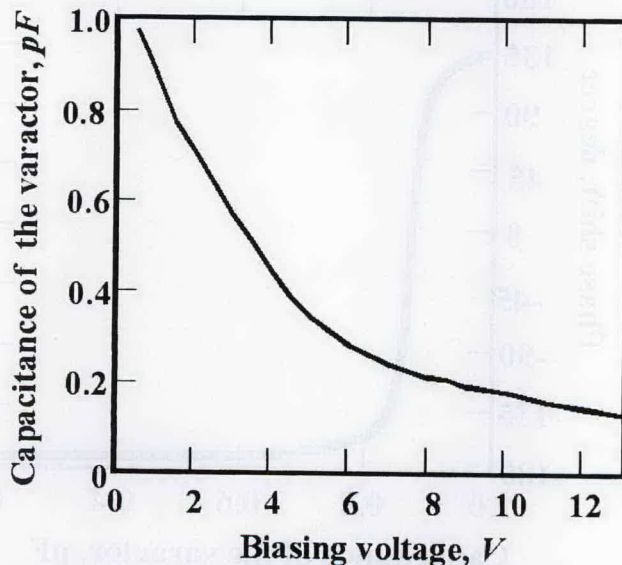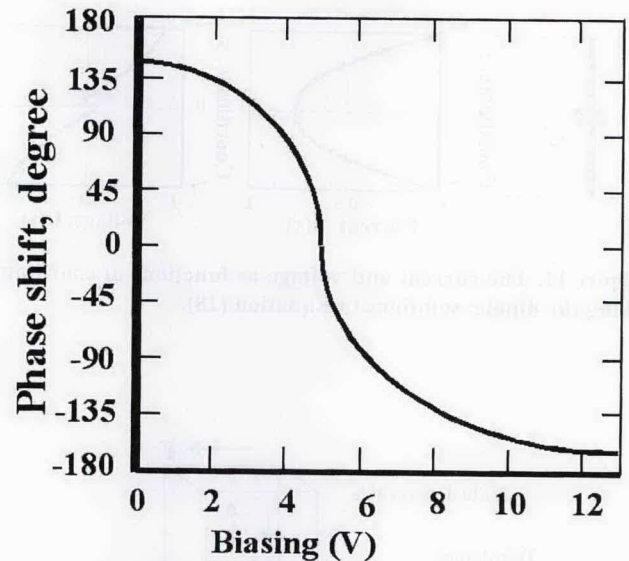

Figure 14a. The varactor capacitance as a function the biasing voltage: a simulation with the formulas of the analytical model.
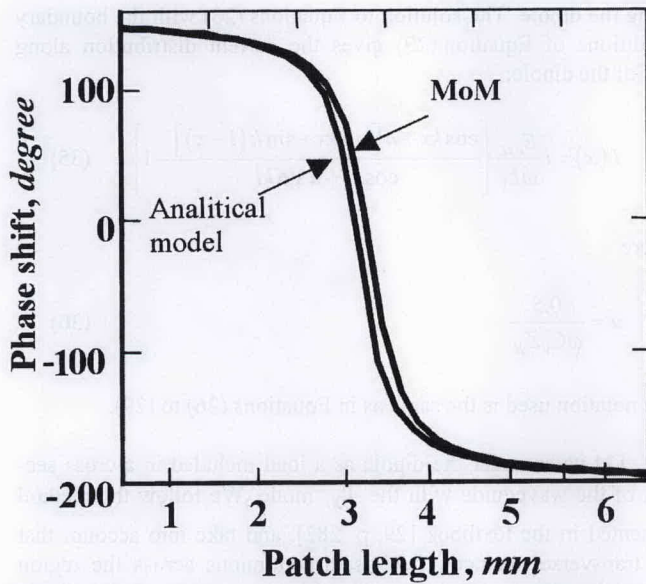
60

Figure 15. A comparison of simulations using the MoM and the analytical model for the dipole without a loading capacitor. The phase shift is a function of the dipole's length.

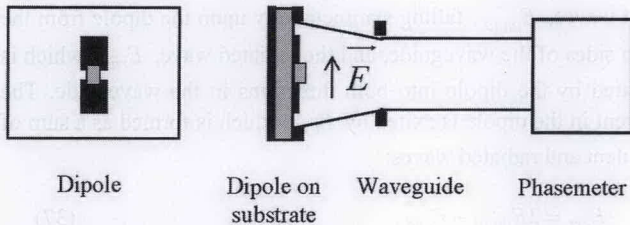Dipole   Dipole on   Waveguide   Phasemeter
            substrate

Figure 16a. The test bench for the measurement of the phase shift and the insertion loss of the reflection-type phase shifter.
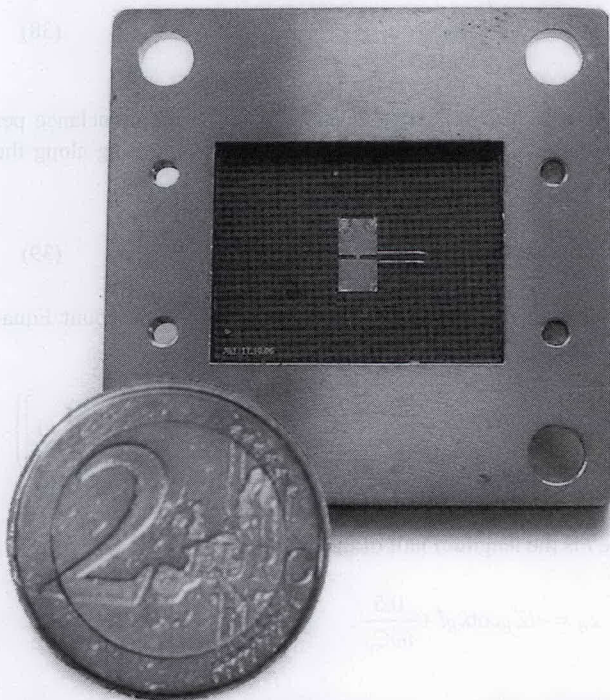

Figure 16b. A photo of a tested phase-shifter cell equipped with the MA46H120 varactor.
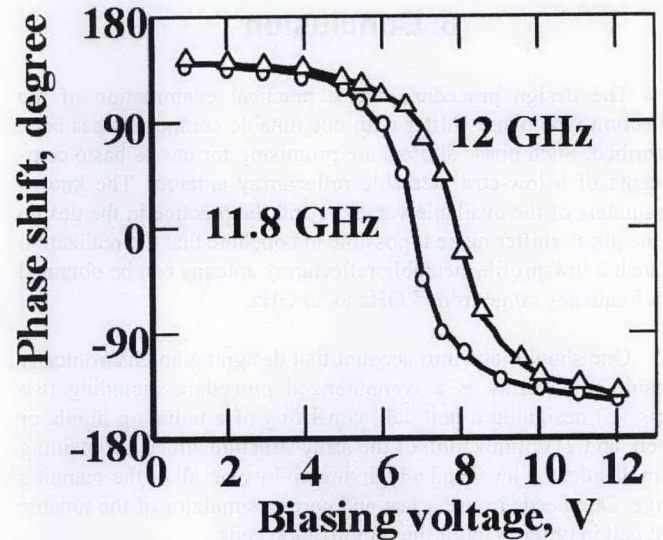

Figure 17a. The results of the measurement of the phase shift of the reflection-type phase shifter as a function the biasing voltage.
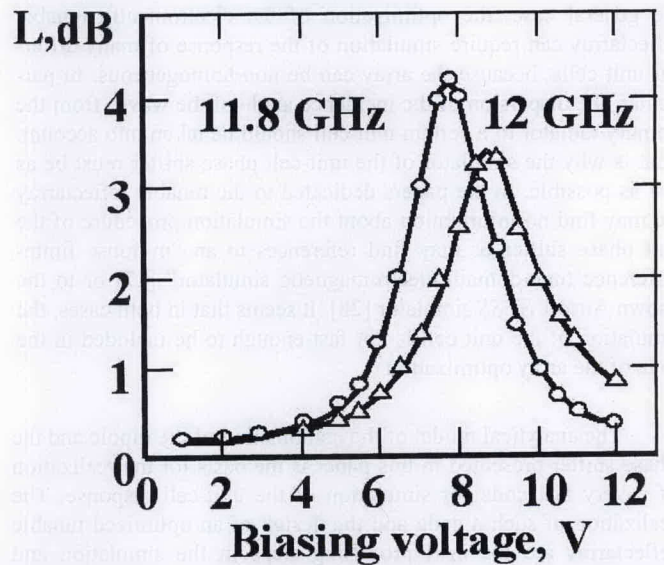

Figure 17b. The results of the measurement of the insertion loss of the reflection-type phase shifter as a function the biasing voltage.

The results of the measurements of the phase shift and the insertion loss of the reflection-type phase shifter are presented in Figures 17a and 17b. The measurements were performed at frequencies of 11.8 GHz and 12 GHz. A MACOM varactor, MA46H120, was used. The capacitance of the varactor was varied from $C_{min} = 0.18\,\text{pF}$ to $C_{max} = 0.9\,\text{pF}$. The series resistance in the equivalent circuit of the varactor was $R = 2.7$ ohms. The dimensions of the dipole were $2l = 8\,\text{mm}$ and $w = 3.5\,\text{mm}$. The substrate had a thickness of $H = 1\,\text{mm}$ and a dielectric permittivity of $\varepsilon_d = 2.8$.

The measured data (Figures 17a and 17b) were in good agreement with the simulated data presented in Figures 14b and 14c. A comparison of the model and measurement data shows that the discrepancies in the phase shift were not higher than 15° and the discrepancies in the loss were not higher than 0.5 dB.

6. Conclusion

The design procedure and a practical examination of the reflection-type phase shifter with one tunable component has been described. Such phase shifters are promising for use as basic components of a low-cost steerable reflectarray antenna. The known parameters of the available varactors and the practice in the design of the phase shifter make it possible to conclude that the realization of such a low-profile steerable reflectarray antenna can be obtained in a frequency range from 5 GHz to 35 GHz.

One should take into account that designing an electronically tunable reflectarray is a computerized procedure including two parts: 1.) designing a unit cell, consisting of a radiating dipole or patch, and 2) optimization of the array structure aimed at obtaining a small sidelobe level and a high directivity over all of the scanning range. One needs to use a fast and correct simulator of the tunable unit cell in order to tailor the optimization code.

The authors of [27], in which all parts of the modeling and design of an electronically tunable reflectarray were considered, wrote about "the future optimization" of the antenna designed with respect to the sidelobe level and the "unaccounted power loss." In the general case, the optimization of the electronically tunable reflectarray can require simulation of the response of many different unit cells, because the array can be non-homogeneous. In particular, the dispersion of the incidence angle of the waves from the primary radiator to a certain unit cell should be taken into account. That is why the simulator of the unit-cell phase shifter must be as fast as possible. In the papers dedicated to the tunable reflectarray we may find no information about the simulation procedure of the unit phase shifter or may find references to an "in-house finite-difference time-domain electromagnetic simulator" [27] or to the known Ansoft *HFSS* simulator [28]. It seems that in both cases, the simulation of the unit cell is not fast enough to be included in the code of the array optimization.

The analytical model of the combination of the dipole and the phase shifter presented in this paper is the basis for the realization of a very fast code for simulation of the unit-cell response. The realization of such a code and the design of an optimized tunable reflectarray are the next promising steps in the simulation and design of electronically tunable reflectarrays suitable for wide commercial application.

7. Acknowledgments

8. Appendix:
The Transformation Coefficient Between
the Dipole and the T_{00} waveguide mode.

Equation (30), for the transformation coefficient n_0, was obtained on the basis of the solution of Equations (28) with the boundary conditions of Equation (29) for the current distribution

along the dipole. The solution to Equations (28) with the boundary conditions of Equation (29) gives the current distribution along half of the dipole:

$$I(x) = i\frac{E_{ext}}{\omega L_1}\left\{\frac{\cos kx + a\left[\sin kx + \sin k(l-x)\right]}{\cos kl + a\sin kl} - 1\right\}, \quad (35)$$

where

$$a = \frac{0.5}{\omega C_v Z_B}. \quad (36)$$

The notation used is the same as in Equations (26) to (29).

Let us consider the dipole as a load included in a cross section of the waveguide with the T_{00} mode. We follow the method presented in the textbook [29, p. 282], and take into account that the transverse magnetic field is discontinuous across the region where the dipole is placed. The imaginary part of the dipole impedance represents the net reactive energy stored in the field of the evanescent modes in the waveguide. We consider the excitation of the current at the dipole by the incident T_{00} wave and the excitation of the T_{00} wave radiated by the dipole. We introduce the incident waves, E_{incid}, falling symmetrically upon the dipole from the both sides of the waveguide, and the radiated wave, E_{rad}, which is emitted by the dipole into both directions in the waveguide. The current in the dipole is exited by E_{ext}, which is formed as a sum of incident and radiated waves:

$$E_{ext} = 2E_{incid} - E_{rad}. \quad (37)$$

The power emitted by both halves of the dipole and transported by the T_{00} wave in two directions in the waveguide can be written as follows:

$$P_1 = E_{rad} 2\int_0^l I(x)dx. \quad (38)$$

Now, we use the following relations between the inductance per unit length, L_1, the wavenumber of the wave traveling along the dipole, k_B, and the dipole characteristic impedance, Z_B:

$$\omega L_1 = k_B Z_B. \quad (39)$$

After integration of Equation (38) and taking into account Equation (36), we obtain

$$P_1 = E_{rad} 2E_{ext}l\frac{1}{z_B}\frac{1}{k_B}\left\{\frac{1}{k_B l} - \frac{1}{\tan k_B l} + \frac{0.5}{\omega C_v Z_B}\left[\frac{\tan(k_B l/2)}{k_B l/2} - 1\right]\right\}, \quad (40)$$

where l is the length of half of the dipole, and

$$z_B = -iZ_B \cot k_B l + \frac{0.5}{i\omega C_v}. \quad (41)$$

We then replace z_B by z_D in the form of Equation (27). We take into account that the dipole consists of two symmetrical parts, and

that the impedance of the tunable varactor includes the small inductive impedance of constructive components and the resistance responsible for the loss. Thus, Equation (40) can be represented as follows:

$$P_1 = E_{rad} E_{ext} \frac{4l^2}{z_D(f,C_v)} \frac{1}{k_B l} \left\{ \frac{1}{k_B l} - \frac{1}{\tan k_B l} \right.$$
$$\left. + \frac{0.5}{\omega C_v Z_B} \left[\frac{\tan(k_B l/2)}{k_B l/2} - 1 \right] \right\}. \quad (42)$$

At the same time, the power radiated by the dipole can be written in the form

$$P_2 = 2E_{rad}^2 \frac{1}{Z_0} L^2, \quad (43)$$

where L is the cross-sectional size of the virtual waveguide (Figure 10), and $Z_0 = 120\pi$ ohms.

On equating the radiated power given by Equations (42) and (43) ($P_2 = P_1$), we obtain

$$2E_{rad} \frac{1}{Z_0} = E_{ext} \frac{1}{z_D(f,C_v)} \frac{4l^2}{L^2} \frac{1}{k_B l} \left\{ \frac{1}{k_B l} - \frac{1}{\tan(k_B l)} \right.$$
$$\left. + \frac{0.5}{\omega C_v Z_B} \left[\frac{\tan(k_B l/2)}{k_B l/2} - 1 \right] \right\}. \quad (44)$$

Using Equation (37), we may rewrite Equation (44) as follows:

$$E_{rad} \frac{2}{Z_0} = (2E_{incid} - E_{rad}) \frac{n_0^2}{z_D(f,C_v)}, \quad (45)$$

where the following notation is used:

$$n_0 = \frac{2l}{L} \sqrt{\frac{1}{k_B l}} \sqrt{\frac{1}{k_B l} - \frac{1}{\tan(k_B l)} + \frac{0.5}{\omega C_v Z_B} \left[\frac{\tan(k_B l/2)}{k_B l/2} - 1 \right]}. \quad (46)$$

Remembering that we introduced the symmetrical incident waves, E_{incid}, falling upon the dipole from both sides of the waveguide, and the radiated waves, E_{rad}, we introduce the symmetrical reflected waves, E_{ref}, traveling into both sides from the dipole:

$$E_{ref} = E_{incid} - E_{rad}. \quad (47)$$

Thus, the reflection coefficient for the symmetrical waves in the waveguide can be defined as

$$\Gamma = E_{ref} / E_{incid}. \quad (48)$$

Eliminating E_{rad} from Equations (45) and (47), we find that

$$\Gamma = \frac{2\frac{1}{n_0^2} z_D(f,C_v) - Z_0}{2\frac{1}{n_0^2} z_D(f,C_v) + Z_0}. \quad (49)$$

The characteristic impedance of the waveguide with the T_{00} wave is 120π ohms.

For symmetrical waves, the doubled impedance shunting the waveguide must be included in the expression for the reflection coefficient [29]. The dipole placed in the waveguide can be considered as a shunt circuit with an impedance of

$$Z_{shunt}(f,C_v) = \frac{1}{n_0^2} z_D(f,C_v), \quad (50)$$

where n_0 has the meaning of the transformation coefficient. Thus, Equation (30) in the text of the paper is substantiated as Equation (50) of the Appendix. The equivalent admittance of the dipole coupled with the T_{00} wave should be written in the form that is used in Equation (31), in correspondence with Figure 12.

9. References

1. D. M. Pozar, S. D. Targonski, and H. D. Syrigos, "Design of Millimeter Wave Microstrip Reflectarrays," *IEEE Transactions on Antennas and Propagation*, **AP-45**, 2, February 1997, pp. 287-296.

2. J. Huang and J. Pogorzelski, "A Ka-Band Microstrip Reflectarray with Elements Having Variable Rotation Angles," *IEEE Transactions on Antennas and Propagation*, **AP-46**, May 1998, pp. 650-656.

3. P. Kabacik, "Design Constraints of Low-Sidelobe Microstrip Phased Arrays," *Microwave and Optical Technology Letters*, **17**, 2, February 1998, pp. 107-111.

4. D. Sievenpiper, J. Schaffner, B. Loo, G. Tangonan, R. Harold, J. Pikulski, and R. Garcia, "Electronic Beam Steering Using a Varactor-Tuned Impedance Surface," IEEE International Symposium on Antennas and Propagation *Digest*, **1**, 2001, pp. 174-177.

5. J. A. Encinar, "Design of Two-Layer Printed Reflectarrays Using Patch of Variable Size," *IEEE Transactions on Antennas and Propagation*, **AP-49**, 10, October 2001, pp. 1403-1410.

6. W. Menzel, D. Pilz, and M. A.- Tikrit, "Millimeter-Wave Folded Reflector Antenna with High Gain, Low Loss, and Low Profile," *IEEE Antennas and Propagation Magazine*, **44**, 3, June 2002, pp. 25-29.

7. O. G. Vendik and M. D. Parnes, *Scanning Reflect-Array Antenna*, 112960 US PTO # 60/751107,12.15.05, patent pending.

8. J. H. Schaffner, R. Y. Loo, D. F. Sievenpiper, F. A. Dolezal, G. L. Tangonan, J. S. Colburn, J. J. Lynch, J. J. Lee, S. W. Livingston, R. J. Broas, and M. Wu, "Reconfigurable Aperture Antennas Using

RF MEMS Switches for Multi-Octave Tunability and Beam Steering," IEEE International Symposium on Antennas and Propagation *Digest*, **1**, 2000, pp. 321-324.

9. J. H. Schaffner, D. F. Sievenpiper, R. Y. Loo, J. J. Lee, and S. W. Livingston, "A Wideband Beam Switching Antenna Using RF MEMS Switches," IEEE International Symposium on Antennas and Propagation *Digest*, **3**, 2001, pp. 658-661.

10. Dan Sievenpiper "Tunable Impedance Surfaces for Low-Cost Beam Steering and Conformal Antennas," Progress in Electromagnetics Research Symposium, PIERS 2006, Cambridge, USA, March 26-29, 2006, p. 133.

11. S. V. Hum, M. Okoniewski, and R. J. Davies, "Realizing an Electronically Tunable Reflectarray Using Varactor Diode-Tuned Elements," *IEEE Microwave and Wireless Components Letters*, **15**, June 2005, pp.422-424.

12. L. Boccia, F. Venneri, G. Amendol, and G. Di Massa, "Application of Varactor Diodes for Reflectarray Phase Control," IEEE International Symposium on Antennas and Propagation *Digest*, **3**, June 2002, pp. 132-135.

13. M. Riel and J.-J. Laurin, "Design of a C-Band Reflectarray Element with Full Phase Tuning Range Using Varactor Diodes," IEEE International Symposium on Antennas and Propagation *Digest*, **3A**, July 2005, pp. 622-625.

14. R. R. Romanofsky, "Unique Issues and Features of a Scanning Reflectarray Antenna Based on Ferroelectric Thin Film Phase Shifters," Progress in Electromagnetics Research Symposium, PIERS 2006, , Cambridge, USA, March 26-29, 2006, p. 134.

15. M. D. Parnes, O. G. Vendik, and V. D. Korolkov, "Design of a Steerable Reflect-Array Antenna with Semiconductor Tunable Varactor Diodes," Progress in Electromagnetics Research Symposium, PIERS 2006, Cambridge, USA, March 26-29, 2006, pp. 130-132.

16. nGimat Co., "A Low Cost Analog Phase Shifter Product Family for Military, Commercial and Public Safety Applications," *Microwave Journal*, **49**, 3, March 2006, p. 152.

17. I. B. Vendik, O. G. Vendik, E. L. Kollberg, "Commutation Quality Factor of Two-State Switching Devices," *IEEE Transactions on Microwave Theory and Techniques*, **MTT-48**, 5, May 2000, pp. 802-808.

18. O.G. Vendik, "Insertion Loss in Reflection-Type Microwave Phase Shifter Based on Ferroelectric Tunable Capacitor," *IEEE Transactions on Microwave Theory and Techniques*, **MTT-55**, 2, February 2007, pp. 425-429.

19. S. K. Koul and B. Bhat, "Microwave and Millimeter Wave Phase Shifters," in S. K. Koul and B. Bhat (eds.), *Semiconductor and Delay Line Phase Shifters*, Norwood, MA, Artech House, 1991.

20. R. J. Mailloux, *Phased Array Antenna Handbook*, Norwood, MA, Artech House, 1994.

21. K. C. Gupta, Ramesh Garg, and Rakesh Chadha, *Computer-Aided Design of Microwave Circuits*, Norwood, MA, Artech House, 1981.

22. Yu. Ya. Yurov, "Engineering Electrodynamics," (lecture aids), Leningrad Electrical Engineering Institute, 1975 (in Russian).

23. C. A. Balanis, *Advanced Engineering Electromagnetics*, New York, John Wiley & Sons, 1989.

24. J. J. Wang, *Generalized Moment Methods in Electromagnetics*," New York, John Wiley & Sons, 1991.

25. P. Russer, *Electromagnetics in Microwave Circuit and Antenna Design for Communication Engineering*, Norwood, MA, Artech House, 2003.

26. T. Itoh, "Spectral Domain Immitence Approach for Dispersion Characteristics of Generalized Printed Transmission Lines," *IEEE Transactions on Microwave Theory and Techniques*, **MTT-28**, 7, July 1980, pp. 733-736.

27. S. V. Hum, M. Okoniewski, and R. J. Davice, "Modeling and Design of Electronically Tunable Reflectarray," *IEEE Transactions on Antennas and Propagation*, **AP-55**, 8, August 2007, pp. 2200-2210.

28. M. Riel and J.-J. Laurin, "Design of an Electronically Beam Scanning Reflect-Array Using Aperture-Coupled Elements," *IEEE Transactions on Antennas and Propagation*, **AP-55**, 5, May 2007, pp. 1260-1266.

29. R. E. Collin, *Foundations for Microwave Engineering, Second Edition*, New York, McGraw-Hill, 1992.

Introducing the Feature Article Authors
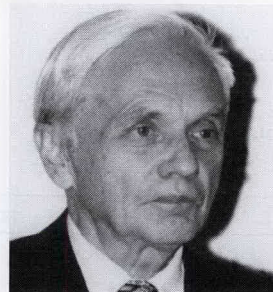
Orest G. Vendik was born in Leningrad in 1932. He received Diploma of Radio Engineer, PhD, and Doctor of Science degrees in 1954, 1957, and 1966, respectively, all from Leningrad Electrical Engineering Institute (now St. Petersburg Electrotechnical University). In 1967-68, he was a researcher on leave at Surrey University (London). He worked at St. Petersburg Electrotechnical University as a Professor of the Department of Applied Physics (1964-1969), and the Head of the Department of Electron-Ion Technology (1969-1989). He is now a Professor of the Department of Physical Electronics and Technology of the same university. During 1992-2002, he periodically worked at Chalmers University of Technology (Sweden) as an invited professor.

His general research interests have been in solid-state electronics, the theory of antennas, and microwave physics. He is the author of five books, and an author of and contributor to more than 250 papers in Russian and international journals. His citation index is more than 2000. Prof. Vendik is a recipient of the USSR State Prize for Science and Technology (1988); Soros Professor Grant winner, Soros Foundation (1994); and was named a Man of

Science of Russian Federation (1999). He has been a member of the St. Petersburg Association of Scientists since 1989, and a member of the IEEE since 1992.

Michael Parnes received his MS in Radio Engineering and his PhD from St. Petersburg Electrotechnical University, Russian Federation, in 1980 and 1990, respectively. Starting from 1980, he worked in the antenna laboratory of the Research Institute as an engineer. Michael has published in a number of journals, and holds a few patents within the radio/antenna production industry. He currently works on microstrip planar antennas as Chief Scientist Officer of MPA Company. His research interests include smart antennas, phased arrays for communication, and radar. ⊕

Correction

The following corrections should be made to the article by Pyotr Ya. Ufimtsev, "New Insight into the Classical Macdonald Physical Optics Approximation," *IEEE Antennas and Propagation Magazine*, **50**, 3, 2008, pp. 11-20:

In Equation (32), the plus sign should be replaced by a minus sign.

The second sentence below Equation (41) should read as follows:

It follows from Equation (40) that the shadow radiation generated separately by these parts of the object is equal to zero in the related specular directions ($\Theta = \pi - \gamma$ or $\Theta = 2\pi - \gamma$).

Correction

The following changes should be made to the article by John W. Arthur, "The Fundamentals of Electromagnetic Theory Revisited," *IEEE Antennas and Propagation Magazine*, **50**, 1, February 2008, pp. 19-65. In the case of citations, the corrected citation is shown.

Location	Change
p. 19, Author's affiliation	Include "University of Edinburgh"
§1.1, p. 20, ¶3, ℓ15	[9; pp. 241-242; 10, vol. 1, pp. 179-181]
§1.2, p. 21, ¶3, ℓ4	[14, pp. 89-95; 15 pp. 84-87 and 100-104; 16, pp. 150-158]
§2.1, p. 23, ¶1, ℓ8	[23, pp. 262-263; 24, p4.11; 14, pp. 155 and 241; 25, p. 503; 26-30; 31, p. 9.3]
§2.12.5, p. 29, ¶2, ℓ8	[39, p.18 and p. 27; 22, p. 153; 45, p. 276]
§2.5, p. 23, ¶1, ℓ5	[10, vol. 2, p. 27]
§2.9.4, p. 26, ¶3, ℓ6	[3, vol. 2, p. 275]
§3.1.1, p. 33, ¶2, ℓ3	[23; 48; 49, p. 14;1, vol. 1, p. 422]
§3.1.1, p. 34, ¶1, ℓ11	[3, vol. 2, p. 240].
§4, p. 40, ¶1, ℓ9	[10, vol. 2, pp. 1-23],
§5, p. 48, ¶2, ℓ3	[22, pp. 380-382; 9, pp. 78-80; 47, pp. 486-495; 56].
§6.6, p. 54, ¶1, ℓ 6 and ℓ 15	[33, IEV 121-11-19]
§6.6, p. 54, ¶1, ℓ8	[33, IEV 121-11-69]
§6.6, p. 54, ¶1, ℓ14 & ¶4, ℓ5	[33, IEV 121-11-56]
§6.6, p. 54, ¶3, ℓ7	[7, p. 453]
§6.6, p. 54, ¶3, ℓ7 and ¶4, ℓ10	[33, IEV 121-11-40]
§6.8, p. 55, ¶1, ℓ3	[67; 45, pp. 70 and 241],
§6.8, p. 56, ¶3, ℓ9	[23, p. 230; 3, vol. 2, pp. 197-198 and 271-276].
§6.13, p. 59, Figure 12, ℓ7	B_{cav} should read B_{int}
§10.3, p. 62, ¶1, "Equation (45)"	Replace with "Equation (46)"
p. 63, references 54 and 73	Remove **34**